International Journal of Engineering

A New Comparative Method to Evaluate the Fracture Properties of Laminated Composite

M.H. Heydari*, N. Choupani

Department of Mechanical Engineering, Sahand University of Technology, Tabriz, Iran

P A P E R   I N F O

A B S T R A C T

In this paper a new method to determine the fracture properties and strain energy release rate for carbon-polyester composite has been introduced. Fracture characteristics such as: critical stress intensity factor and critical strain energy release rate for mode I, mode II and mixed mode loading were determined using Arcan type specimen. 130 layers of carbon fiber polyester woven composite with each of 0.2mm thickness were put on each other. Theoretical studies to determine strain energy release rate were done using three methods: Corrected Beam Theory (CBT), Compliance Calibration Method (CCM), Virtual Crack Closure Technique (VCCT), and results were recorded and compared with the results from experimental and numerical attempts. Critical loads were recorded through experimental attempts then applied to the finite element software. Results were recorded and compared with each other to determine the best method. Results show that CCM and VCCT determine strain energy release rate value closer to J-integral in comparison with corrected beam theory. Finally, the fracture surfaces were examined by scanning electron microscope to gain insight intothe failure responses that shows the fracture surface for mode II is rougher than the fracture surface for mode I and mixed mode.

NOMENCLATURE

a	Crack length	P_C	Critical load
G	Strain energy release rate	CBM	Corrected beam method
G_I	Mode-I or opening-mode strain energy release rate	CCM	Compliance calibration method
G_{II}	Mode-II or shearing-mode strain energy release rate	VCCT	Virtual crack closure technique
G_T	Total strain energy release rate	DCB	Double cantilever beam
G_C	Critical strain energy release rate	ENF	End notch flexure
J	J-integral	MMF	Mixed-mode flexure
K	Stress intensity factor	ELS	End load split
K_I	Mode-I or opening-mode stress intensity factor	SLB	Single leg bending
K_{II}	Mode-II or shearing-mode stress intensity factor	CLS	Crack lap shear
K_C	Critical stress intensity factor	EDT	Edge delamination tension
P	Applied load	MMB	Mixed mode bending

1. INTRODUCTION

Carbon-fiber reinforced plastics, such as polyester and epoxy resins, have recently become dominant advanced materials over conventional materials such as aluminum or steel, because of their high stiffness, high strength, and reasonable price. In fact,composites are being increasingly used in structures requiring high specific strength and stiffness, such as in the automotive, aerospace, electronic devices and marine industries [1, 2].

Failure in laminated composites has been one of the major subjects being studied extensively in recent years. Delamination in plies is the most common failure mode in composite laminates that can cause fiber breakage

*Corresponding Author's Email: Mhh.Mechanic@Gmail.Com(M.H. Heydari)

and reduction in life of the composite. In fact, it is known that delamination can cause significant stiffness losses and promotes overall failure. Interfacial cracking between layers or delamination can be a result of impact, or bearing load in bonded joints, high shear and peeling stress concentrations or any other sources of significant interlaminar stresses. Currently, interlaminar fracture toughness or critical energy release rate of a composite is measured using different methods [3, 4]. Ullah, et al. [5] studied the damage in woven GFRP composites under large-deflection bending through experimental and numerical methods under large-deflection bending. Chen and Dai [6] investigated the interlaminar delamination growth of laminated circular plates under in-plane loads and movable boundary conditions based on von-Karman plate theory.

Delamination can occur under all three basic modes of crack growth: under mode I, mode II, and mode III or under combinations of these modes (mixed mode). It is important, therefore, to improve the knowledge of delamination growth both theoretically and experimentally. The most straightforward way is studying different methods to determine strain energy release rate and fracture phenomena. During the last decades, many methods have been proposed to determine fracture properties in these three modes, such as Double Contilever Beam (DCB), End Notch Flexure (ENF), End Load Split (ELS), Mixed-mode Bending (MMB), and Arcan specimen. Mode I fracture has been extensively studied by the DCB test according to ASTM D-5528-94a [7, 8]. For mode II, three major tests are currently employed: ENF, ELS and the Four-Point End Notched Flexure. ENF test has been widely used for the determination of the mode II delamination toughness of laminated composites. The main advantage of this test is that it is carried out by a simple three-point bending test. Several authors have also reported that ENF test allows only the determination of initial values but not of resistance curves [9, 10]. An anisotropic nonlinear cohesive model based on continuum damage mechanics to predict the mixed-mode delamination of composite laminates through numerical attempts was proposed by Liu[11]. A delamination method was proposed by Wanget al. [8] to characterize Mode I and Mode II delamination in carbon fiber/epoxy (CF/EP) composite laminates through interrogation of guided waves activated by piezoelectric actuators in a pitch–catch configuration. Peng et al. [12] developed a solution based on experimental studies to investigate the fatigue delamination growth of multidirectional laminates with 45°/−45° fracture interface under three mixed mode I/II ratios. Kumar et al. [13]performed a finite element analysis to study the partial delamination modeling in composite beams using a finite element method. An investigation into the mixed mode fracture of steel fiber reinforced concrete (SFRC) beams with one percent volume fraction of steel fiber was carried out by Kazemi and Zakeri[14].

Various attempts have been made to characterize interlaminar fracture toughness under mixed-mode loading conditions, but mostly beam type specimens have been used [15, 16]. Some of these includes: the mixed-mode flexure test, the end loaded split specimen, the Single Leg Bending (SLB) specimen, the Crack Lap Shear (CLS) test, the Edge Delamination Tension (EDT) specimen, and the Asymmetric Double Cantilever Beam (ADCB). The MMB test is relatively easy to execute and provides an easy alteration of mixed-mode ratio only changing the lever length of the apparatus. The MMB was developed by Reeder and Crews (1990) and has been used for mixed-mode I/II interlaminar fracture characterization of artificial [17, 18]. Figure 1 presents the DCB, ENF, and MMB test methods.

2. TEST PROCEDURE

This paper seeks to determine critical interlaminar stress intensity factors (K_c) and strain energy release rate (SERR) for mode I (G_I), mode II (G_{II}) and mixed mode (G_{I+II}) loading conditions through experimental and numerical attempts. All experimental studies were performed using modified version of Arcan specimen. One of the main advantages of Arcan fixture is its special geometry that makes it possible to determine mode I ($\alpha=0°$), mode II($\alpha =90°$) and mixed mode ($\alpha=45°$) critical force and fracture properties (Figure 2). The Arcan test specimen was developed to produce a uniform state of plane-stress in solid specimens. Originally, Arcan et al. [18] proposed this test as a monolithic Arcan specimen, where the grips and the butterfly specimen are cut out of a single plate. Thus, no joints were necessary between the butterfly specimen and the grips. While the Arcan apparatus was primarily suited for testing of fiber-reinforced materials, recent developments have shown that the Arcan test can also be used with adhesives, isotropic materials and composite materials [18, 19]. The main component of the Arcan apparatus is a butterfly specimen, which is joined on either side to two half-circular grips (Figure 2). The grips are connected to a universal testing machine at the top and bottom, respectively.

Strain energy release rate were determined with four methods: J-integral, CCM, CBT, and VCCT and results were compared. Critical loads were determined through experimental attempts and applied to ABAQUS [20] software to determine critical strain energy release rate using J-integral, and opening displacement at crack region were recorded to determine strain energy release rate with CCM and CBT. Strain energy release rate were determined using VCCT method as well after detecting the nodal forces with finite element software.

At the end, the fracture surfaces of the composite under different mixed mode loading conditions were examined by optical and scanning electron microscopy to gain insight into the failure responses.
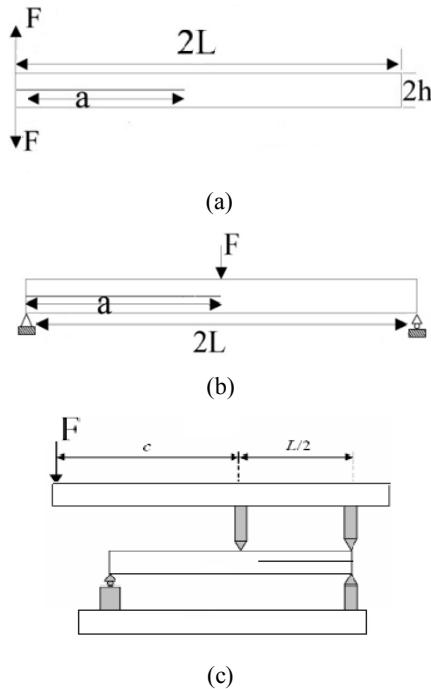

(a)

(b)

(c)

Figure 1. Schematic representationof (a) DCB (b) ENF and (c) MMB test methods
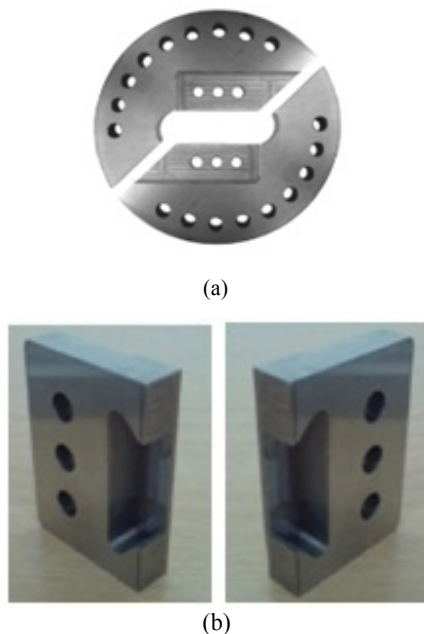

(a)

(b)

Figure 2. (a) Arcan fixture and(b) supporters

3. THEORETICAL STUDIES

3. 1. Corrected Beam Method The proposed data reduction scheme was developed and applied to Arcan test to determine strain energy release rate. It is based on beam theory and crack equivalent concepts.The fracture energy in mode I can now be obtained using the Irwin–Kies equation [8, 21]:

$$J_{IC} = \frac{P^2}{2B} \frac{dC}{da} \tag{1}$$

where P is load, B is the specimen width, a is the crack length and C is compliance given by [18]:

$$C = \frac{\delta}{P} \tag{2}$$

where δ is the opening displacement. The opening displacement for the samples with the crack placed on the mid plane is [21]:

$$\delta = \frac{2Pa^3}{3EI} \tag{3}$$

where I is the moment of inertia. Using Equations (1) and (3), the strain energy release rate can be obtained from following expression [21]:

$$G_{Ic} = \frac{3P\delta}{2Ba} \tag{4}$$

For mode II crack propagation, assuming a cubic relationship between the compliance (C) and the measured crack length, is [8]:

$$C = D + ma^3 \tag{5}$$

where D and m are constants. G_{IIc} can now be obtained from the following relationship [8]:

$$G_{IIC} = \frac{3P^2 ma^2}{2B} \tag{6}$$

3. 2. Compliance Calibration Method When the cracked specimen is subjected to load, as long as there is no crack propagation and the elastic behavior is linear, the load-displacement relation is [1]:

$$U = CP \tag{7}$$

where C is the compliance of specimen, it means the compliance is the slope which referred to as the stiffness and the inverse of stiffness is called the compliance. Another compliance expression is [1]:

$$C = Ka^n \tag{8}$$

where n is the slope of $\ln(C)$ versus $\ln(a)$ curve. Therefore, the energy release rate expression becomes [1, 21]:
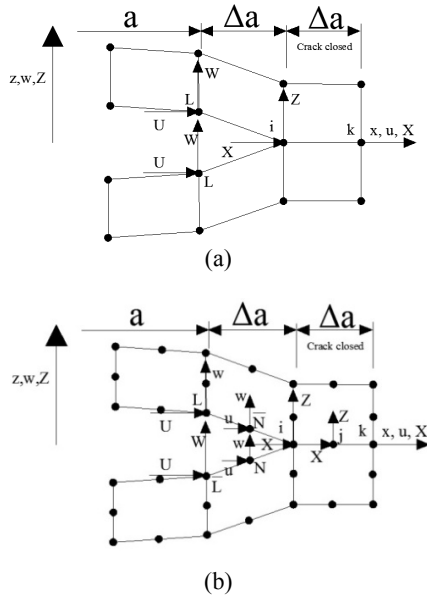
$$G = \frac{nP\delta}{2ab} \tag{9}$$

(a)

(b)

Figure 3. (a) VCCT method for 4-node elementsand (b) VCCT method for 8-node elements

3. 3. Virtual Crack Closure Technique

One of the most commonly used fracture mechanics approach is the Virtual Crack Closure Technique (VCCT), originated from the finite crack extension method and the virtual crack extension method. The VCCT is based on nodal forces and displacements near the crack tip. In this technique, the four elements adjacent to the tip should preferably have the same size (Figure 3). Shokrieh and Zeinedini[22] developed a novel method for calculation of strain energy release rate of asymmetric double cantilever laminated composite beams under VCCT and MBT methods. The authors used the virtual crack closure technique to obtain the energy release rates. During the last decades, the VCCT has successfully been used to obtain both the total strain energy release rate and the mode mixity for cracks in homogeneous and composite materials and adhesive bonded joints. The strain energy release rate for mode I and mode II for a 4-node element are as follow [23, 24]:

$$G_I = -\frac{1}{2\Delta a}.Z_i(w_L - w_{L^*})$$
$$G_{II} = -\frac{1}{2\Delta a}.X_i(u_L - u_{L^*})$$

(10)

whereΔa is the crack tip element length, $X_i$andZ_i are the crack tip forces at node i. The relative displacements at the crack tip can be determined by displacement of the nodes at the upper crack plane;w , u; and displacement of the nodes at the lower crack plane; w, u (at node L) (Figure 3-a). The strain energy release rate for mode I and mode II for an 8-node element are [23]:

$$G_I = -\frac{1}{2\Delta a}.[Z_i.(w_L - w_{L^*}) + Z_j.(w_m - w_{m^*})]$$

(11)

$$G_{II} = -\frac{1}{2\Delta a}.[X_i.(u_L - u_{L^*}) + X_j.(u_m - u_{m^*})]$$

whereX_i, Z_i are the crack tip forces at node I; Z_J and$X_j$aremiddle forces behind the crack at node J (Figure 3-b).

3. 4. Mixed Mode I/II Delamination

Delamination growth under mixed mode I and mode II conditions is studied by the CLS specimen, the MMB specimen and the Arcan fixture. The MMB test is the superposition of the two previous tests, and it allows any combination of mode I and mode II loadings to be obtained. The expressions for mode I and mode II energy release rate components are [25]:

$$G_I = \frac{12(a + h|\Delta_I|)^2 P_I^2}{B^2 h^3 E_L}$$

(12)

$$G_{II} = \frac{9(a + 0.42h|\Delta_I|)^2 P_{II}^2}{16 B^2 h^3 E_L}$$

E_L is the longitudinal modulus and $\Delta_I$isgiven by [24]:

$$\Delta_I = \sqrt{\frac{E_L}{11 G_{LR}}\left[3 - 2\left(\frac{\Gamma}{1+\Gamma}\right)^2\right]}$$

(13)

And [24]:

$$\Gamma = 1.18\frac{\sqrt{E_L E_R}}{G_{LR}}$$

(14)

where E_R and $G_{LR}$are the radial and shear modulus, respectively. The mode ratio can be obtained from [17, 25]:

$$\frac{G_I}{G_{II}} = \frac{4}{3}\left(\frac{3c - L}{c + L}\right)^2\left(\frac{a + h\Delta_I}{a + 0.42\Delta_I h}\right)^2$$

(15)

3. 5. Stress Intensity Factor

It is assumed that the composite specimens are orthotropic linear elastic material. The strain energy release rates for orthotropic material can be calculated from the following relationships [18]:

$$G_I = \frac{K_I^2}{E_I} \quad G_{II} = \frac{K_{II}^2}{E_{II}}$$

(16)

where E_I and $E_{II}$are effective moduli, and K_I and K_{II} are mode-I and mode-II stress intensity factors, respectively. For plane strain conditions, effective moduli E_I and E_{II} are defined as [26, 27]:

$$E_I = \frac{\sqrt{2}}{b_{11}}.\left(\left(\frac{b_{22}}{b_{11}}\right)^{1/2} + \frac{2b_{12} + b_{66}}{2b_{11}}\right)^{-1/2}$$

(17)

$$E_{II} = \left(\frac{2}{b_{11}b_{22}}\right)^{1/2}.\left(\left(\frac{b_{22}}{b_{11}}\right)^{1/2} + \frac{2b_{12} + b_{66}}{2b_{11}}\right)^{-1/2}$$

where the terms of the constants b_{ij} are defined in terms of the following non-zero entries a_{ij} of the orthotropic compliance matrix [26]:

$$b_{ij}=a_{ij}(a_{i3}a_{j3}/a_{33})\ldots\ldots(I,j=1, 2, 3, 4, 5, 6) \qquad (18)$$

4. NUMERICAL ATTEMPTS

During the last decades, finite element modeling has become a useful tool to analyze fracture properties for composite material and adhesive bonded joints. In the present paper, all numerical attempts were carried out using interaction J-integral method performed in ABAQUS finite element software with various crack lengths under critical loads [20].

All connection pins are assumed to be rigid in comparison with composite specimen, in numerical 2D modeling specimen and Arcan fixture are modeled stick together (Figure 4-a) and in 3d modeling Arcan fixture and composite specimen are modeled as it is shown in Figure 4-b. So, in the finite element analysis, the specimen–fixture system was treated as one continuous solid with two regions of different thickness and material properties. Crack was laid in mid plane of specimen with specific length. To get suitable finite element results, the model was partitioned and meshed using eight nodes collapsed quadrilateral element and the mesh was refined around the crack tip.

To obtain $1/\sqrt{r}$ fracture singularity, the elements around the crack tip were focused on the crack tip and the mid-side nodes were moved to a quarter point of each element side (Figure 4-c).

In 2D modeling, loads were applied as concentrated nodal loads on appropriate hole, and in 3D modeling, to have more precise results; loads were applied on the surface of hole in each mode as a distributed load. The Arcan fixture has two sides, and one side is under the loading condition and other side is completely fixed, as a boundary condition.

To determine the critical strain energy release rate, critical loads were determined through experimental works and applied to model to determine final results. Based on the definition of the J-integral, the interaction integrals can be directly related to the stress intensity factors as follow [20]:

$$K=4\pi B.J_{int} \qquad (19)$$

where B is called the pre-logarithmic energy factor matrix. $K=[K_I, K_{II}, K_{III}]^T$ and $J_{int}=[J^I_{int}, J^{II}_{int}, J^{III}_{int}]^T$. In linear elastic fracture mechanics, the J integral indicates the total strain energy release rate, $J=G_T = G_I +G_{II}$ where G_I and G_{II} are the energy release rates associated with the mode-I and mode-II stress intensity factors.
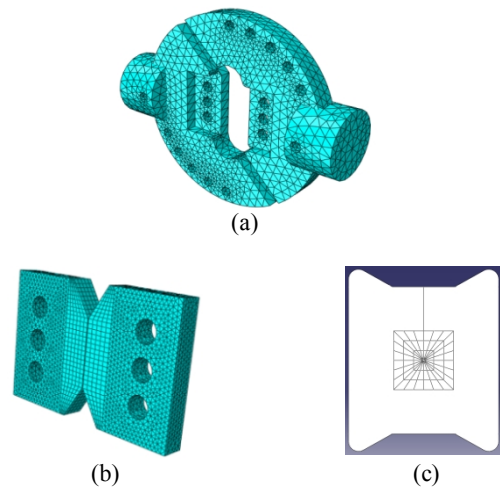

(a)

(b) (c)

Figure 4 (a), (b). 3D modeling of Arcan fixture and specimenand **(c)** 2D modeling and mesh pattern of specimen and contour around the crack tip
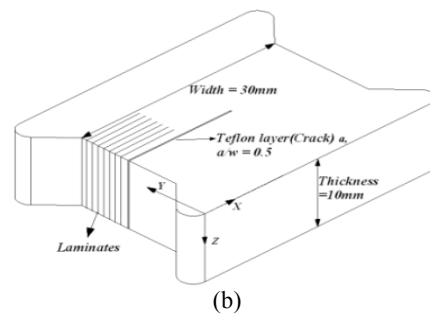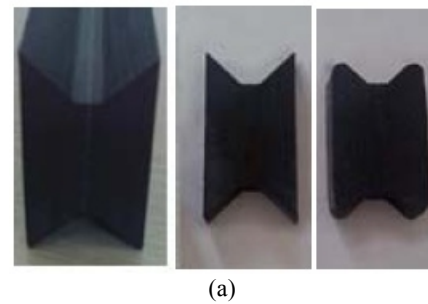

(a)

(b)

(c)

Figure 5. (a) Preparation process of specimen,**(b)**schematic of specimen and**(c)**non adhering film as a pre crack

TABLE 1. Elastic properties of carbon-polyester laminated composite (GPa) [27]

E_1	E_2	E_3	G_{12}	G_{13}	G_{23}	ν_{12}	ν_{13}	ν_{23}
87	87	12	7	3.6	3.6	0.02	0.4	0.4

5. EXPERIMENTAL SET-UP

5. 1. Material Description Laminated composite specimens were prepared by hot pressing at a temperature of 100°C higher than the T_g of the matrix resin and consisted of 130 plies of cross-ply carbon-polyester woven laminates each of 0.2 mm thickness to form a block. The starter delamination was produced using a none adhering film, inserted at the mid-ply, with a thickness of 0.1mm. The blocks were cut with a diamond wheel and machined to the dimensions of approximately 30mm×10mm×26mm, finally machined into specimen with the geometry given in Figure 5-b. The composite tested in this work is woven carbon fibre reinforced thermoplastic which had been dried for about 2.5 hours at 120°C and had not been exposed toany other treatment before use. Table 1 shows the mechanical properties of carbon-polyester composite,where the subscript 1 stands for the fiber direction, 2 is perpendicular to the fiber direction, but in the plane of the ply, and 3 is the direction perpendicular to the plane of the ply.

5. 2. Testing Procedure In this study, a modified version of Arcan specimen was made for the mixed-mode fracture test of carbon-polyester specimens, which allows mode-I, mode-II, and mixed mode loading to be tested with the same test specimen configuration. The Arcan test specimen was developed to produce a uniform state of plane-stress in solid specimens. Originally, Arcan et al. [18] proposed this test as a monolithic Arcan specimen, where the grips and the butterfly specimen are cut out of a single plate. Thus, no joints were necessary between the butterfly specimen and the grips.Arcan apparatus was primarily suited for the biaxial testing of fiber-reinforced materials, recent developments have shown that the Arcan test can also be used with adhesive, isotropic materials and composite material [18, 19].

A simple and compact fracture mechanics specimen was used for the determination of fracture toughness under mode-I, mode-II and mixed-mode loading conditions. The loading device is simply installed in the universal testing machine. All tests were done at room temperature, and under displacement control rate of 0.5mm/min. Load versus opening deflection displacement (P-δ) curves were recorded during loading and the critical loads were determined. In order to minimize the error in theproject, all tests were repeated three times for each mode. Figure 6 shows the typical Arcan fixture and loading device.

6. RESULTS and DISCISSIONS

6. 1. Experimental and Numerical Results As mentioned above, all experimental studies were carried out using Arcan specimen under room temperature with a rate control of 0.5 mm/min to reduce the dynamic error effects. In order to have data more accurate, all tests were performed three times for each mode.
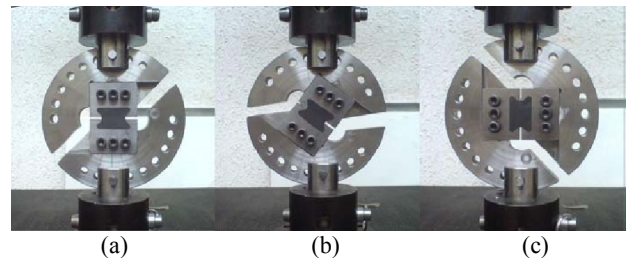

Figure 6. Loading device and test setup. (a) pure mode-I(α=0°), (b) mixed-mode(α=45°)and (c) pure modeII (α=90°)
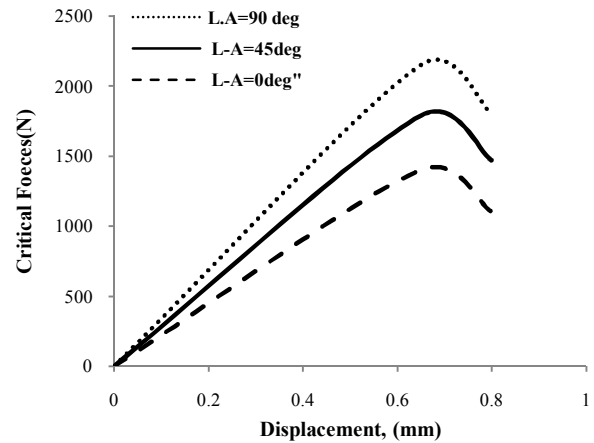

Figure 7. P-δ curve determined experimentally

TABLE 2. Critical loads (N) and standard deviation for different modes with crack length of 15mm

Loading angle	First time (N)	Second time (N)	Third time (N)	Average (N)	Std.
Mode I (L.A=0°)	1420	1390	1410	1406	12.8
Mixed mode (L.A=45°)	1810	1785	1805	1800	10.8
Mode II (L.A=90)	2110	2205	2200	2170	43.6

Numerical attempts were carried out using finite element software ABAQUS under critical loads. Strain energy release rate were determined using four methods: J-integral, VCCT, CCM, and CBT. Results have been compared and recorded. Figure7 shows a typical load versus opening deformation curve for specimens from minimum to critical load. From Figure7, it can be seen that the load increased until a maximum value was reached and then gradually decreased. Also the fracture was found to be completely brittle with the load–displacement curves. The load increased sharply initially and gradually decreased after the peak force occurred. The decrease in load was accompanied by a gradually growing crack. Critical loads for mode I, mode II, and mixed mode are presented in Table 2. From this table it can be seen that critical loads in opening mode (mode-I) are smaller than critical loads in mixed mode and second mode. This means specimen shows less resistance in opening mode and more resistance in mixed-mode; finally the maximum resistance takes place in shearing mode. The average values of critical fracture loads were used to determine the critical mixed-mode stress-intensity factors and strain energy release rates data. Gning et al.[28] investigated the through-thickness strength of glass/epoxy butterfly-shaped specimens under pure shear and biaxial loadings using an Arcan device. The results showed that there is no regular change in failure loading when loading angles vary from 0° to 90°. So the minimum of failure load is 1954 and the maximum is 3769 at loading angles of75° and 0°, respectively. In contrast, in the present work there was a regular increase in failure loading when loading angle changed from 0° to 90°.

All numerical attempts were carried out with finite element software ABAQUS through two and three dimensional modeling using J-integral methods. Since the stiffness of the Arcan pins is higher than the stiffness of the composite specimen, it is assumed that the Arcan pins to be rigid in the analysis. The connection between the fixture and specimen is idealized by rigid and continuous joints. Critical loads, determined in experimental section, were applied to FE software to determine critical strain energy release rate with J-integral method. Opening displacement at crack region was recorded numerically to get critical strain energy release rate with CCM and CBT. Nodal forces were recorded numerically, as well, to determine critical strain energy release rate with VCCT. VCCT, CBT, and CCM have gained lots of popularity recently to determine the strain energy release rate because these methods present advantages relatively to the classical methodologies, such as it does not require crack measurement during propagation and it accounts for the root rotation at the clamping point. In order to summarize the results, all final results determined through four methods CBT, CCM, VCCT, and J-

integral and relative error are shown in Table 3 for mode I, and in Table 4 for mode-II as a function of crack length to form R curve.

It is clear to see that strain energy release rate increases as the crack length increases and at the smaller crack lengths G_c increases smoothly, when the crack propagates further G_c increases sharply. This rising R curve is a commonly observed feature in these tests, and is attributed to the growth of a zone of nested fibres bridging the crack faces. Both of CCM and CBT (Equation (4)) methods depend on rigorous crack monitoring during propagation, which is very difficult to perform experimentally. However, numerically it is easy to do crack evolution. CBT underestimates the value of G_{IIc}. The CBT depends on the real crack length measured experimentally. The CCM is based on specimen compliance calibration, which is affected by the energy being dissipated in the fracture plastic zone. However, in view of the used cubic polynomial approach, the fracture energy equation also depends on the real crack length. Moreover, it should be emphasized that the CCM requires crack length measurements during the propagation. The CCM presents a slight difference, explained by polynomial fitting difficulties. From Table 3, it could be seen that the CBT method presents a smaller G for all tested specimens. In fact, this method does not include crack length corrections in order to account for root rotation and shear effects, which explains the underestimated results. Table 3 also shows that as the crack length increases the differences between CBT and experimental method increases too, it means that CBT shows more errors in crack length ratiosabove 0.5. For the CCM and VCCT, good agreements with the experimental value were obtained with less error. It is important to notice that for all methods strain energy release rate increases as the crack length increases. The minimum of strain energy release rate in mode-I is 6.5 J/m^2 with CBT method when crack length ratio is 0.1, and the maximum of G_I is 461 J/m^2; using VCCT attempt when the crack length ratio is 0.8.

Table 4 presents the strain energy release rate for second mode (mode II) and relative errors in each methods. It is clear to see that from Tables 3 and 4, similar results could be obtained and the average amount of G_I is higher than G_{II}. For mode II, the minimum strain energy release rate is 4.3 J/m^2 in CBT method and the maximum of strain energy release rate for mode-II (G_{II}) is 185 J/m^2 using VCCT method. Dharmawan et al.[29] examined the mixed mode fracture toughness of GFRP composites through experimental studies.

In the result section, the authors illustrate the R-curve for DCB specimens. They showed that strain energy release rate increases with the crack length until a stable value was reached at a crack length of about 70 mm. On the other side, in this paper strain energy

release rate increased with the crack length and there was no stability. Due to the strong anisotropy of composite structures, the fracture is usually not a result of pure modeI or pure mode II loading, and the delamination occurs in the mixed mode loading conditions. For this reason, the study of the mixedmode interlaminar fracture toughness is very important. The MMB test can be viewed as a combination of the DCB and the ENF tests. The deformation in the region of the crack tip shows a combination of opening and shear loading modes. The mixed mode fracture results (G_I/G_{II}) determined with Equation 16 are summarized in Table 5 as a function of crack length. It is clear that for crack length ratios less that 0.4, G_I and G_{II} are close to each other and G_I/G_{II} is close to 1, but as the crack length increases, approximately for crack length ratios more than 0.4, the G_I/G_{II} becomes bigger than before.

The variation of strain energy release rate for mode-I and mode II along the width of the specimen with J-integral and VCCT methods are presented in Figures 8, 9. From Figure 8, it can be seen that G_I starts from 125 J/m^2 in the edge of specimen and reaches to 430 J/m^2 in the middle of specimen, and it is clear to notice that G_I shows a tendency to have a sharp variation to get the maximum amount of 430 J/m^2. Another important feature that worth thinking is that for distance less than 4mm from the edge of specimen the J-integral and VCCT results are close to each other, and for distance more than 4mm from the edge there is higher difference between two methods. Figure 9 presents the variation of strain energy release rate for mode-II (G_{II}) versus width of specimen determined through J-integral and VCCT methods. As it can be seen, G_{II} varies smoother than G_I from minimum 120 J/m^2 to maximum 180 J/m^2, and there is a constant difference between two methods.

Characterizing the interlaminar fracture toughness is the most effective factor in determining the fracture of composite materials as failures in composite materials occur mainly due to interlaminar fracture, also called delamination, between laminates. ASTM standards E 399 [30] and D 5045 [31] give some guidance for plane strain mode-I fracture toughness K_{IC} for metals and plastics. No standard requirement exists for the validity of linear elastic fracture mechanics and plane-strain conditions for tests with composites under mixed-mode loading conditions. Therefore, it may be necessary to develop ASTM standardized tests, tailored for use with composites for the Arcan specimen geometry to investigate the role of mixed-mode loading conditions. The strain energy release rates for orthotropic material with the crack line parallel to the principal orthotropic direction which coincides with the fibre orientation can be calculated from the following relationships [18]:

$$G_I = \frac{K_I^2}{E_I} \qquad\qquad G_{II} = \frac{K_{II}^2}{E_{II}} \qquad\qquad (20)$$

where E_I and $E_{II}$are effective modulus. In this paper mixed mode tests were done using Arcan specimen with α=45°. With special shape of Arcan specimen, critical loads could be determined for mode I (α=0°), mode II (α=90°) and wide range of mixed modes (α=15°, 30°, 45°, 60°, 75°) and strain energy release rates for mixed mode conditions were determined with Equation(16).

Stress intensity factors for mode I and mode II were determined with Equation(20), and are summarized in Tables 6-8 with relative errors in each method. From Table 6, it could be seen that as the crack length increases the stress intensity factor for mode I (K_I) increases too that the minimum value in experimental attempt is 0.598 MPa√m when the crack length ratio (a/w) is 0.1, and the maximum value is 4.492 MPa√m when the crack length ratio is 0.8. Another important feature that worth thinking is that CCM and VCCT methods giveresults closer to experimental attempts in comparison with CBT.
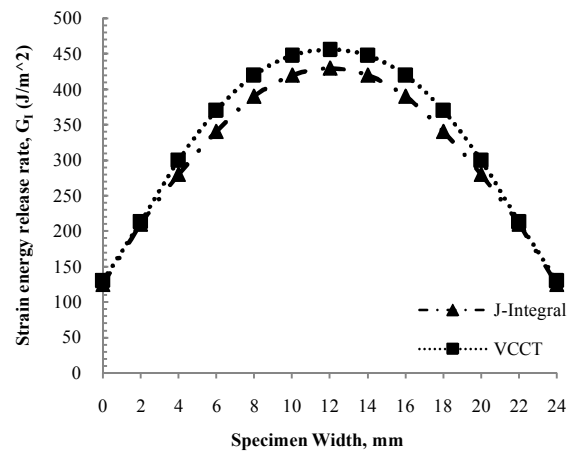

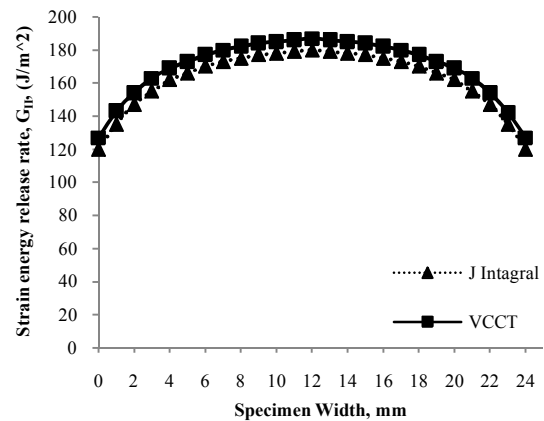**Figure8.** $G_I$versus width of specimen, a/w= 0.8

Figure 9. G_{II}versus width of specimen, a/w=0.8

Table 7 presents the critical stress intensity factors for mode II (K_{II}). It can be seen that the same result as Table 6 could be gotten. The minimum value in experimental attempt is 0.549 MPa√m when crack length ratio (a/w) is 0.1 and the maximum value is 2.890 MPa√m when crack length ratio is 0.8. Table 8 shows the mixed mode stress intensity factor for Carbon-Polyester versus different crack length ratio using with K_I/K_{II} equation. As it can be seen, the K_I/K_{II} relationship is always bigger than one and for crack length ratio smaller than 0.4 K_I and K_{II} are close to each other. Nikbakht, et al. [19] carried out an experimental attempt to study the strain energy release rate and fracture toughness of Carbon/ Epoxy composite using Arcan specimen.

In their study, the failure loads increased with the loading angle, the same results were reached in the present work so that stress intensity factor for mode I (K_{IC}) remained almost constant, and stress intensity factor for mode II (K_{IIC}) increased when loading angles change from 0° to 90°.

TABLE 3. Strain energy release rate in mode I (G_I, J/m^2) for carbon-polyester with crack length=15 mm

Crack length ratio, a/w	Experimental	CCB		CCM		VCCT	
	G_I	G_I	Error- %	G_I	Error- %	G_I	Error- %
0.1	7.7	6.5	15.6	7.4	4.00	8	3.8
0.2	15.5	11.7	24.5	16	3.2	17	9.6
0.3	28.5	26	8.7	30	5.3	30	5.2
0.4	65	55.7	14.3	68	5.00	60	7.7
0.5	100	87	0.13	105	0.05	97	3
0.6	155	125	19.3	151	2.6	161	3.8
0.7	233	200	14.2	230	1.2	250	7.3
0.8	435	420	3.4	458	5.2	461	6.0

TABLE 4. Strain energy release rate in mode II (G_{II}, J/m^2) for carbon-polyester with crack length=15 mm

Crack length ratio, a/w	Experimental	CCB		CCM		VCCT	
	G_{II}	G_{II}	Error- %	G_{II}	Error- %	G_{II}	Error- %
0.1	6.5	4.30	33	6.00	8	7.1	9
0.2	14.1	10.2	27	15.2	7	16.1	14
0.3	26.1	21.8	16	28.7	9	28	7
0.4	39.6	37.0	6	41.1	3	43.2	9
0.5	61.2	58.6	4	63.3	3	64.4	5
0.6	92.8	85.2	8	94.2	1	96.1	3
0.7	134.2	123.1	8	141.2	5	148.2	10
0.8	180	168	6	175	2	185	2

TABLE 5. Strain energy release ratio in mixed mode, (G_I/G_{II}) for carbon-polyester with crack length=15 mm

Crack length ratio, a/w	Experimental	CCB		CCM		VCCT	
	G_I/G_{II}	$G_I/_{II}$	Error- %	G_I/G_{II}	Error- %	G_I/G_{II}	Error- %
0.1	1.18	1.51	2	1.23	4	1.12	5
0.2	1.10	1.15	4	1.05	4	1.05	4
0.3	1.09	1.19	9`	1.07	2	1.07	1
0.4	1.64	1.50	8	1.65	0.6	1.39	15
0.5	1.63	1.48	9	1.66	2	1.50	8
0.6	1.67	1.47	11	1.60	4	1.67	0
0.7	1.74	1.62	6	1.63	6	1.69	3
0.8	2.65	2.50	5	2.68	1	2.49	6

TABLE 6. Critical stress intensity factor in mode I (K_I, MPa$\sqrt{m}$) for carbon-polyester with crack length=15 mm

Crack length ratio, *a/w*	Experimental	CCB		CCM		VCCT	
	K_I	K_I	Error- %	K_I	Error- %	K_I	Error- %
0.1	0.598	0.549	8	0.586	2	0.609	1.8
0.2	0.848	0.722	14	0.862	2	0.888	4.7
0.3	1.149	1.100	4	1.180	2.6	1.18	2.6
0.4	1.736	1.607	7	1.776	2.3	1.66	4.3
0.5	2.154	2.009	6	2.207	2.4	2.12	1.5
0.6	2.682	2.408	10	2.647	1.3	2.73	1.8
0.7	3.288	3.046	7	3.267	0.6	3.40	3.4
0.8	4.492	4.415	2	4.610	2.6	4.62	2.8

TABLE 7. Critical stress intensity factor in mode II (K_{II}, MPa$\sqrt{m}$) for carbon-polyester with crack length=15 mm

Crack length ratio, a/w	Experimental	CCB		CCM		VCCT	
	K_{II}	K_{II}	Error- %	K_{II}	Error- %	K_{II}	Error- %
0.1	0.549	0.447	18.5	0.528	3.8	0.574	4.5
0.2	0.809	0.690	14.7	0.840	3.8	0.864	6.7
0.3	1.100	1.005	8.6	1.154	5	1.140	3.6
0.4	1.355	1.310	3.5	1.381	1.9	1.416	4.5
0.5	1.685	1.650	2.0	1.714	1.7	1.729	2.6
0.6	2.075	1.990	4.0	2.091	0.7	2.111	1.7
0.7	2.495	2.393	4	2.560	2.6	2.622	5
0.8	2.890	2.792	3.4	2.850	1.4	2.930	1.4

TABLE 8. Critical stress intensity factor in mixed mode K_I/K_{II} for carbon-polyester with crack length=15 mm

Crack length ratio, *a/w*	Experimental	CCB		CCM		VCCT	
	K_I/K_{II}	K_I/K_{II}	Error- %	K_I/K_{II}	Error- %	K_I/K_{II}	Error- %
0.1	1.089	1.228	12.7	1.11	2.0	1.060	2.7
0.2	1.048	1.046	2.0	1.026	2.0	1.027	2.0
0.3	1.044	1.094	4.7	1.022	2.1	1.035	0.8
0.4	1.281	1.227	4.2	1.286	4.8	1.178	8.0
0.5	1.278	1.217	4.8	1.290	0.9	1.227	4.0
0.6	1.292	1.21	6.3	1.266	2.0	1.195	7.5
0.7	1.318	1.273	3.4	1.276	3.2	1.300	1.4
0.8	1.554	1.581	1.7	1.617	4.0	1.578	0.1

6. 2. Failure Surfaces of Mixed-mode Interlaminar Fracture   The mode-I interlaminar fracture surfaces were examined using a Scanning Electron Microscope (SEM). The SEM of fracture surfaces of the mode-I specimens are shown in Figures 10a, b and c. Figure 10a and b show the fractograph of the mode-I fracture of the initiation area taken just beyond the pre crack insert film of the carbon-polyester composite. So, the fractures surfaces show the first increment of interlaminar crack growth which corresponds to the measured fracture toughness. The mode-I fracture surface is indicative of a brittle cleavage

failure with relatively smooth and flat matrix fracture and shows debonding between fibre and matrix(A), which would explain the low mode-I fracture toughness. Figure 10c shows the fractograph of a mode-I fracture of the propagation area. Its characteristic is overall flatness on the matrix fracture (B).

SEM micrographs show that the fracture surfaces of the woven carbon-polyester composite change with mixed-mode ratio. Figures 11a, b and c show the interlaminar fracture surfaces at mixed-mode loading conditions ($\alpha = 45°$) for the woven carbon-polyester composite. At pure mode-I the fracture surface was very

flat indicating a brittle cleavage fracture which would explain the low mode-I fracture toughness. As mode-II loading contribution is added, the fracture surfaces become rougher as seen in the micrograph taken just after the pre crack insert film under mixed-mode (α = 45°) loading conditions.

Troughs (C) and hackles (D) have appeared where fibres have been pulled away from the matrix indicating interfacial failure. Hackles are regions of the matrix deformation between adjacent fibres that are lifted up parallel to one another and tend to slant in the same direction over the entire surface. Fracture surfaces showed evidence of some distributed pores and voids (E). Some fibres were peel out which show the presence of mode-I component (F). The characteristic of the fracture surface is the traces of fibres in the resin regions combined with voids and debonded fibres.

The observations of the mode-II fracture surfaces were carried out with scanning electron microscopy. SEM of fracture surfaces of the mode-II specimens are shown in Figure 12a, b and c. A scanning electron micrograph of the area at the rear of the crack tip of the fracture surface of the mode-II specimen is shown in Figure 12a and b. Everywhere on the fracture surface of the specimens, broken fibres (G) were observed, as the marks of fibre-matrix debonding and hackles accompanied by fragmentation of the matrix phase (H). Hackles are regions of the matrix deformation between adjacent fibres that are lifted up parallel to one another and tend to slant in the same direction over the entire surface.

Figure 12c shows the fractograph of a mode-II fracture at the propagation area. Its characteristic is numerous inclined hackles of the matrix fracture and troughs (K) where fibres have been pulled away (N) from the matrix indicating interfacial failure. However, due to the large relative motion in mode-II loading, the fracture surface was rough and more voids, debonded particles and traces of bridging fibres were detected (P). The presence of voids with a smeared appearance indicates that ductile crack propagation conditions are favoured with respect to the mode-I specimen case because an increased shear deformation is allowed.

Hojoet al. [32] investigated the interlaminar fracture toughness and delamination fatigue crack growth behavior for carbon fiber (CF)/epoxy laminates with the self-same epoxy interleaf through experimental studies. As a part of experimental studies, SEM of fracture surface under mode-I and II wasdetermined. For the base laminates (Figure 13a), a large number of carbon fibers and their pullout traces were observed. The areal ratio of the interfacial fracture was about 30%. On the other hand, about 90% of the fracture surface was covered with resin in the case of 50 lm-epoxy-interleaved laminates (Figure 13b). The morphology of the resin part shows brittle fracture with little trace of the plastic deformation.

Figures 14(a) and (b) show the SEMs of the static fracture surfaces of the base laminates and those of the 50 lm epoxy-interleaved laminates for mode II loading, respectively. Typical hackle markings were observed for both laminates. The height and interval of the hackle markings for the 50 lm-epoxy interleaved laminates are much larger than those for the base laminates [32].
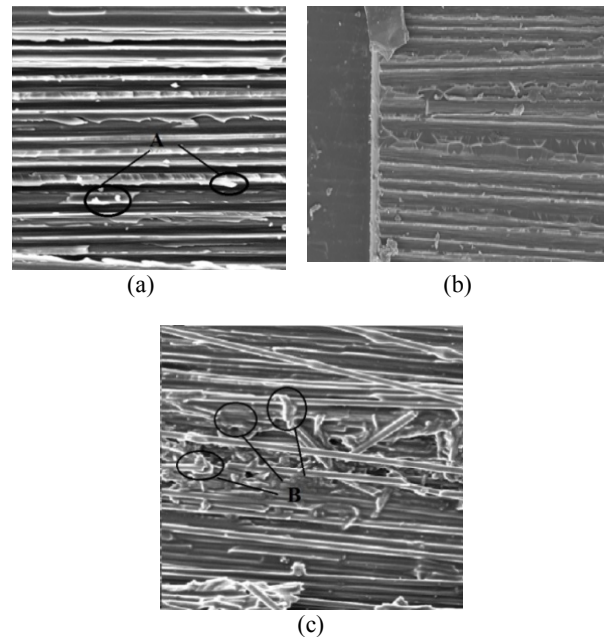

(a)   (b)

(c)

Figure 10. (a,b) Initiation fracture surfaceand (c) propagation fracture surface of pure opening mode

(a)   (b)
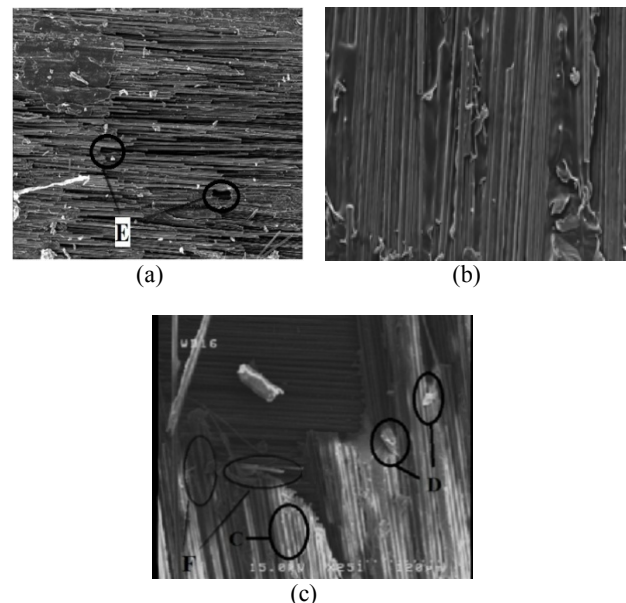
(c)

Figure 11. (a, b) Initiation fracture surfaceand (c) propagation fracture surface of mixed mode loading of 45°
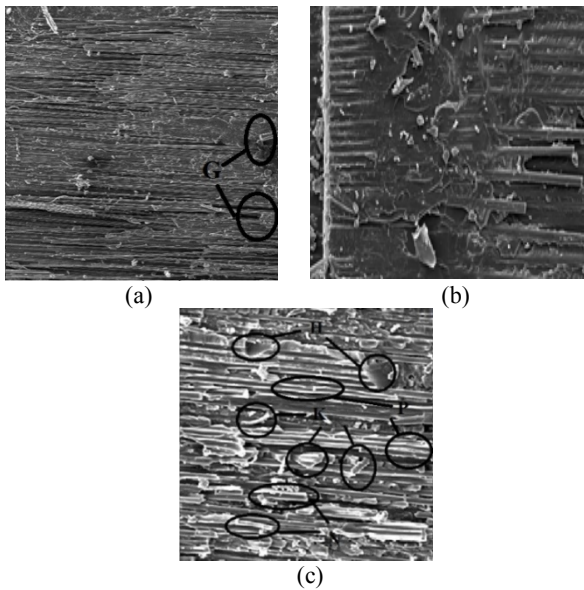
(a)   (b)

(c)

Figure 12. (a, b) Initiation fracture surfaceand (c) propagation fracture surface of pure shearing mode
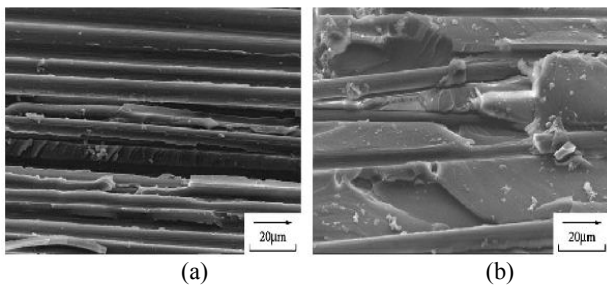

(a)   (b)

Figure 13. (a) Scanning electron micrographs of fracture surfaces under mode I loading and (b) base laminates static fracture [32].
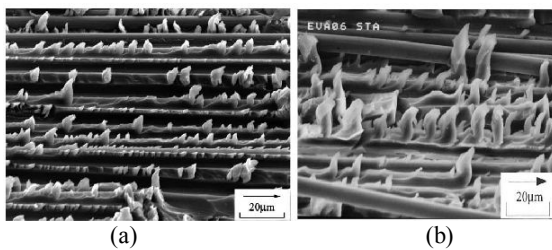

(a)   (b)

Figure 14. (a) Scanning electron micrographs of fracture surfaces under mode II loadingand (b) base laminates static fracture [32]

Yadavet al. [33] studies the fracture toughness behaviour of carbon fibre epoxy composite with Kevlar reinforced interleave. SEM micrographs for baseline (controlled) sample show a good adhesion between fibre and matrix, as shown in Figure 15, which is quite common and referred as hackles. This is caused by in-plane shear with tilt of hackle indicating the crack propagation direction.Figures 16 and 17 show that

Kevlar fibres bend and are interlocking with other underneath fibres causing the fibre pull out breakage due to tensile stress during delamination. The fibrils of Kevlar fibres pass through carbon fibre because fibres may have acted as bridge crossing the fracture surface during delamination. Further, Figure 18 shows that detached carbon fibre from fracture plane may have contributed to crack interface bridging [33].
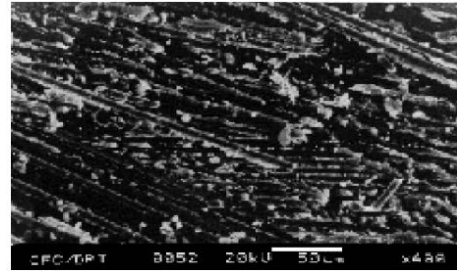

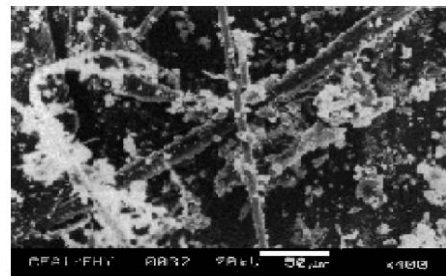**Figure15**. SEM Microphotograph of baseline (controlled) sample [33]

Figure 16. SEM microphotograph of 0.5 mg Kevlar reinforced samples [33]
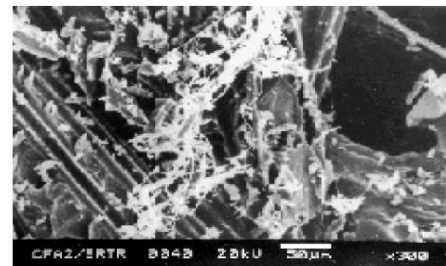

Figure 17. SEM microphotograph of 1.0 mg Kevlar reinforced samples [33]
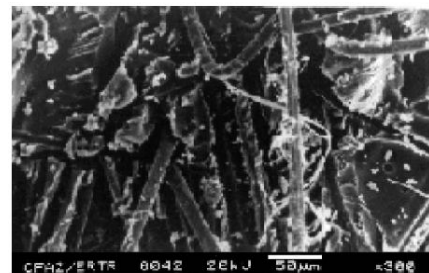

Figure 18. SEM microphotograph of 1.5 mg Kevlar reinforced samples [33]

7. CONCLUSION

In this paper the mode I, mode II, and mixed mode fracture properties, such as fracture toughness and strain energy release rate were determined using experimental and numerical methods. A modified version of Arcan specimen was employed to conduct a mixed mode test using the special test loading device and recording the critical loads. As a numerical part, finite element software ABAQUS was used. Arcan fixture and composite specimen were modeled in two and three dimensions. Critical loads, determined experimentally, were applied to the software to determine the strain energy release rate with J integral, crack tip opening displacements (δ), and nodal forces.

Strain energy release rate were detected through Corrected Bead Theory, Compliance Calibration Method, and Virtual Crack Closure Technique with theoretical and numerical attempts. Answers were compared with the strain energy release rate determined with J integral to get the best method. Results show that as the crack length increases SERR for mode I and mode II increases too, and CBT shows answers more conservative than other methods. In addition, the strain energy release rate through J integral and VCCT methods in mode I and mode II have been compared and recorded as a graph across the specimen width. Graph shows that the strain energy release rate for mode I tends to have a variation sharper than strain energy release rate for mode II, and reaches the maximum amount at the middle of width.

At the end, the critical stress intensity factors were determined through CBT, VCCT, CCM, and experimental attempts. The fracture surfaces of the woven carbon-polyester composite under different mixed mode loading conditions were examined by scanning electron microscopy to gain insight into the failure responses. The SEM fracture surface observations showed that the mode I fracture surface is indicative of a brittle cleavage failure with relatively smooth and flat matrix fracture and shows only a little debonding between fibre and matrix. As the mode II loading contribution is added, the fracture surfaces become rougher and troughs and hackles appear. Everywhere on the mode II fracture surface of the specimens, broken fibres, troughs and hackles were observed.

8. REFERENCES

1. Gdoutos, E.E., "Fracture mechanics: An introduction", Springer, Vol. 123, (2006).
2. Liu, P. and Zheng, J., "On the through-the-width multiple delamination, and buckling and postbuckling behaviors of symmetric and unsymmetric composite laminates", *Applied Composite Materials*, Vol. 20, No. 6, (2013), 1147-1160.
3. Argüelles, A., Viña, J., Canteli, A. and Lopez, A., "Influence of the matrix type on the mode i fracture of carbon-epoxy composites under dynamic delamination", *Experimental Mechanics*, Vol. 51, No. 3, (2011), 293-301.
4. Shanmugam, V., Penmetsa, R., Tuegel, E. and Clay, S., "Stochastic modeling of delamination growth in unidirectional composite dcb specimens using cohesive zone models", *Composite Structures*, Vol. 102, (2013), 38-60.
5. Ullah, H., Harland, A.R. and Silberschmidt, V.V., "Experimental and numerical analysis of damage in woven gfrp composites under large-deflection bending", *Applied Composite Materials*, Vol. 19, No. 5, (2012), 769-783.
6. Chen, D. and Dai, L., "Delamination growth of laminated circular plates under in-plane loads and movable boundary conditions", *Communications in Nonlinear Science and Numerical Simulation*, Vol. 18, No. 11, (2013), 3238-3249.
7. D5528-94a, American Society for Testing and Materials ASTM Standard, "Test method for mode i interlaminar fracture toughness of unidirectional fiber-reinforced polymer matrix composites", *West Conshohocken*, (2001).
8. Wang, D., Ye, L., Tang, Y. and Lu, Y., "Monitoring of delamination onset and growth during mode I and mode ii interlaminar fracture tests using guided waves", *Composites Science and Technology*, Vol. 72, No. 2, (2012), 145-151.
9. Arrese, A., Carbajal, N., Vargas, G. and Mujika, F., "A new method for determining mode II r-curve by the end-notched flexure test", *Engineering Fracture Mechanics*, Vol. 77, No. 1, (2010), 51-70.
10. Rajabi, A. and Kadkhodayan, M., "An investigation into the deep drawing of fiber-metal laminates based on glass fiber reinforced polypropylene", *International Journal of Engineering-Transactions C: Aspects*, Vol. 27, No. 3, (2013), 349.
11. Liu, P. and Islam, M., "A nonlinear cohesive model for mixed-mode delamination of composite laminates", *Composite Structures*, Vol. 106, (2013), 47-56.
12. Peng, L., Xu, J., Zhang, J. and Zhao, L., "Mixed mode delamination growth of multidirectional composite laminates under fatigue loading", *Engineering Fracture Mechanics*, Vol. 96, No., (2012), 676-686.
13. Keshava Kumar, S., Ganguli, R. and Harursampath, D., "Partial delamination modeling in composite beams using a finite element method", *Finite Elements in Analysis and Design*, Vol. 76, No., (2013), 1-12.
14. Kazemi, M.T. and Zakeri, I., "Mixed mode fracture in reinforced concrete with low volume friction of steel fibers", *International Journal of Engineering*, Vol. 24, No. 1, (2011), 1-18.
15. Shokrieh, M., Heidari-Rarani, M. and Rahimi, S., "Influence of curved delamination front on toughness of multidirectional dcb specimens", *Composite Structures*, Vol. 94, No. 4, (2012), 1359-1365.
16. Gong, X., Hurez, A. and Verchery, G., "On the determination of delamination toughness by using multidirectional dcb specimens", *Polymer Testing*, Vol. 29, No. 6, (2010), 658-666.
17. Bennati, S., Colleluori, M., Corigliano, D. and Valvo, P.S., "An enhanced beam-theory model of the asymmetric double cantilever beam (ADCB) test for composite laminates", *Composites Science and Technology*, Vol. 69, No. 11, (2009), 1735-1745.
18. Heydari, M.H., Choupani, N. and Shameli, M., "Experimental and numerical investigation of mixed-mode interlaminar fracture of carbon-polyester laminated woven composite by using arcan set-up", *Applied Composite Materials*, Vol. 18, No. 6, (2011), 499-511.
19. Nikbakht, M., Choupani, N. and Hosseini, S., "2d and 3d interlaminar fracture assessment under mixed-mode loading conditions", *Materials Science and Engineering: A*, Vol. 516, No. 1, (2009), 162-168.
20. Manual, A.U.s., "Version 6.5, hibbitt, karlsson and sorensen", *Inc., Pawtucket, RI*, (2004).
21. Agius, S.L., Magniez, K.J. and Fox, B.L., "Fracture behaviour of a rapidly cured polyethersulfone toughened carbon fibre/epoxy

composite", ***Composite Structures***,   Vol. 92, No. 9, (2010), 2119-2127.

22. Shokrieh, M. and Zeinedini, A., "A novel method for calculation of strain energy release rate of asymmetric double cantilever laminated composite beams", ***Applied Composite Materials***, (2013), 1-17.

23. De Moura, M., Oliveira, J., Morais, J. and Xavier, J., "Mixed-mode I/II wood fracture characterization using the mixed-mode bending test", ***Engineering Fracture Mechanics***, Vol. 77, No. 1, (2010), 144-152.

24. Shokrieh, M., Rajabpour-Shirazi, H., Heidari-Rarani, M. and Haghpanahi, M., "Simulation of mode I delamination propagation in multidirectional composites with r-curve effects using vcct method", ***Computational Materials Science***, Vol. 65, (2012), 66-73.

25. Ducept, F., Davies, P. and Gamby, D., "Mixed mode failure criteria for a glass/epoxy composite and an adhesively bonded composite/composite joint", ***International Journal of Adhesion and Adhesives***, Vol. 20, No. 3, (2000), 233-244.

26. Heydari, M.H. and Choupani, N., "Effects of thickness on fracture toughness of carbon/polyester composite", ***Key Engineering Materials***, Vol. 471, (2011), 886-891.

27. Choupani, N., "Characterization of fracture in adhesively bonded double-lap joints", ***International Journal of Adhesion and Adhesives***, Vol. 29, No. 8, (2009), 761-773.

28. Gning, P.B., Delsart, D., Mortier, J. and Coutellier, D., "Through-thickness strength measurements using arcan's method", ***Composites Part B: Engineering***, Vol. 41, No. 4, (2010), 308-316.

29. Dharmawan, F., Simpson, G., Herszberg, I. and John, S., "Mixed mode fracture toughness of gfrp composites", ***Composite Structures***, Vol. 75, No. 1, (2006), 328-338.

30. "Astm e399.”standard test method for plane strain fracture toughness and strain energy release rate of metallic materials”. In: Annual book of astm standards. (1983).

31. "Astm d5045, “standard test method for plane strain fracture toughness and strain energy release rate of plastic materials”. In: Annual book of astm standards ", (1995).

32. Hojo, M., Ando, T., Tanaka, M., Adachi, T., Ochiai, S. and Endo, Y., "Modes I and II interlaminar fracture toughness and fatigue delamination of cf/epoxy laminates with self-same epoxy interleaf", ***International Journal of Fatigue***, Vol. 28, No. 10, (2006), 1154-1165.

33. Yadav, S., Kumar, V. and Verma, S.K., "Fracture toughness behaviour of carbon fibre epoxy composite with kevlar reinforced interleave", ***Materials Science and Engineering: B***, Vol. 132, No. 1, (2006), 108-112.

A New Comparative Method to Evaluate the Fracture Properties of Laminated Composite

M.H. Heydari,N. Choupani

Department of Mechanical Engineering, Sahand University of Technology, Postal Code 51335-1996, Tabriz, Iran

چکیده

در این مقاله یک روش جدید برای تعیین خواص شکست و نرخ رها سازی انرژی کرنشی کامپوزیت لایه ای کربن– پلی استر معرفی شده است. پارامترهای شکست نظیر ضریب شدت تنش بحرانی و نرخ رها سازی انرژی کرنشی برای مود یک، مود دو و مودهای مرکب بارگذاری به کمک نمونۀ آرکان بدست آورده شدند. در این مقاله ۱۳۰ لایه کامپوزیت کربن– اپوکسی بافته شده با ضخامت هر لایه ۰/۲ میلیمتر روی یکدیگر قرار داده شد. مطالعات تئوری به منظور بدست آوردن نرخ رها سازی انرژی کرنشی بر اساس سه روش CCM, VCCT, CBT انجام گرفت. در پایان نتایج ثبت شده و با نتایج مطالعات عددی و تجربی مقایسه شدند. به کمک آزمایشات تجربی، بارهای بحرانی از طریق آزمایشات با نرخ بارگزاری ثابت بدست آورده شده و سپس به نرم افزار المان محدود اعمال شدند. مطالعات عددی در محیط نرم افزار آباکوس و روش انتگرال J انجام گرفت. نتایج حاصله از روش های مختلف با هم مقایسه شده و بهترین روش برای تحلیل مشخص شد. نتایج پژوهش بیان می کنند که نرخ انرژی کرنشی بدست آمده از روش های CCM و VCCT در مقایسه با روش CBT به روش انتگرال J نزدیکتر می‌باشد. در پایان، سطوح شکست تحت آزمایشات شکست نگاری به منظور مطالعۀ دقیق سطوح شکست در هر مود قرار گرفت. این تصاویر بیان می‌کنند که سطوح شکست مد دوم از مد یک و مدهای مرکب سخت تر می‌باشد.

doi:10.5829/idosi.ije.2014.27.06c.18